# Behaviour and design of circular hollow section steel columns strengthened by infilling concrete under preload

H.X. Yuan [a,b,*], X.X. Du [a], M. Shokouhian [c], J. Ye [d], B.W. Schafer [b]

[a] *Key Laboratory of Geotechnical and Structural Engineering Safety of Hubei Province, School of Civil Engineering, Wuhan University, Wuhan 430072, PR China*
[b] *Department of Civil Engineering, Johns Hopkins University, Baltimore, MD 21218, United States of America*
[c] *Department of Civil Engineering, Morgan State University, Baltimore, MD 21251, United States of America*
[d] *Department of Civil and Environmental Engineering, Imperial College London, London SW7 2AZ, United Kingdom*

## ARTICLE INFO

## ABSTRACT

The objective of this work is to develop design guidance for existing hollow steel columns that are retrofitted by infilling concrete into the tubes. The primary challenge is the unknown effect of the existing preload on the steel columns prior to the concrete infill. Composite performance and buckling behaviour of circular hollow section (CHS) steel columns strengthened by infilling concrete under preload was experimentally and numerically investigated in this study. A total of 34 CHS steel columns were tested under pin-ended boundary conditions, and the overall buckling failure modes and corresponding ultimate buckling resistances were recorded. Prior to the member testing, material properties of the steel columns and the infilled concrete were attained. By means of the finite element (FE) software package ABAQUS, elaborate FE models for the CHS columns strengthened by infilling concrete were developed and validated against the obtained test results, which were further verified with other available test data. Using the validated FE models, systematic parametric studies were conducted to examine the influences of the major factors affecting the ultimate capacities of the CHS columns strengthened by infilling concrete, including preload ratios, steel and concrete strengths, steel ratios, initial global imperfections, eccentricity ratios and column slenderness ratios. The obtained test and numerical results were therefore utilised to develop design criteria for predicting the overall buckling resistance of CHS steel columns strengthened by infilling concrete. In view of the difficulty of determining the key parameters in practice and the uncertainty of the strengthening process, a new simplified design coefficient was proposed, taking into account the influence of the preload. It has been demonstrated that accurate and reasonable strength predictions can be provided by the proposed design method.

© 2019 Elsevier Ltd. All rights reserved.

## 1. Introduction

Strengthening existing steel structures is often imperative due to additional imposed loads or alterations of primary function [1]. Methods used to reinforce steel structures include welding cover plates [2–4], bonding steel plates or fibre reinforced polymer materials [5–7], external post-tensioning using tendons [8–10]. For steel tubular columns, infilling concrete into the tube columns is another feasible retrofit technique that has little effect on both the appearance and the net area. The infilled concrete benefits from the confining effect provided by the steel tube and may also delay the occurrence of local buckling [11–14]. As a result, the load-carrying capacity of an existing steel tubular column can be significantly enhanced. It is noted that the infilling concrete will introduce additional self-weight to the structural system, yet this can be considered in the retrofitting process, with additional design checks to be conducted. Generally, it would be essential to unload the columns prior to strengthening. However, it is inconvenient and often infeasible to unload the column before strengthening, therefore the strengthening process is carried out while the member is subjected to self-weight and external actions [15–17]. The composite strength and flexural stiffness is sensitive to this existing load; therefore, in this paper, the overall buckling behaviour of circular hollow section (CHS) steel columns strengthened by infilling concrete under preload is investigated.

There have been a number of experimental and numerical studies aiming at exploring the preload effect on the concrete-filled columns. Uy and Das [18] considered the effect of wet concrete loading of steel box section columns during construction by FE modelling, and Han and Yao [19] tested 19 concrete-filled square hollow steel columns subjected to preload and developed design formulae for the calculation of the ultimate strength. Meanwhile, Zha [20] tested a total of 27 concrete-filled CHS columns with various preload ratios, Huang and

\* Corresponding author at: School of Civil Engineering, Wuhan University, Wuhan 430072, PR China.
*E-mail address:* yuanhx@whu.edu.cn (H.X. Yuan).

Chen [21] carried out nine concrete-filled CHS column tests with initial stresses, and Liew and Xiong [22] conducted experimental studies on 11 CHS steel columns infilled with normal concrete and high strength concrete subjected to preloads arising from construction and permanent loads of the building, and then a modified design method was developed. More recently, Patel et al. [23,24] presented numerical studies on both circular and rectangular concrete-filled steel tubular slender beam-columns with preload effects, while Huang et al. [25] reported an experimental study on concrete-filled steel tubular columns with preload ratios of 0, 0.25 and 0.5, and a simplified prediction method for preload reduction effect was proposed. In general, the preload applied on the steel tube, produced by the self-weight and construction imposed loads, such as the working loads and wet concrete, reached around 30% of the column buckling capacity. It has also been suggested that preload up to 60% of the steel tube strength has an insignificant effect on the member capacity [26]. However, the stress ratio in steel tubular columns from existing structures may reach up to 0.80 or higher when considering additional imposed loads as a result of design changes on the building's function. Therefore, a comprehensive research on the influence of higher preload ratios is needed to underpin the design of CHS steel columns strengthened with concrete infill. Moreover, while there is a need for the development of procedure on the efficient retrofitting of steel hollow sections, a new design methodology for predicting the capacity of concrete-filled steel hollow sections subjected to preload is required.

This paper presents a comprehensive experimental programme on overall buckling behaviour of a total of 34 CHS columns involving high preload ratios. The column specimens strengthened by infilling concrete were loaded with pin-ended boundary conditions. FE modelling on the overall buckling behaviour of the tested columns and other available test data was carried out in ABAQUS. Subsequently, parametric studies were conducted to examine the influences of the major factors that affect the overall buckling behaviour of CHS columns. Based upon the obtained test and numerical results, a new design method for predicting the overall buckling resistance of CHS columns strengthened by infilling concrete subjected to preload was developed. The current study also comprises part of the fundamental research work to provide a general revision on the Chinese code for strengthening steel structures [27].

## 2. Experimental programme

### 2.1. Test specimens

A total of 34 CHS steel column specimens were prepared for the experimental programme. The outer diameter ($D$) of the tubular cross-sections was 159.0 mm with a wall thickness ($t$) of 4.0 mm. Three tensile coupons were machined directly from the steel tubes and tested to acquire the average material properties: Young's modulus $E_s = 2.03 \times 10^5$ MPa, yield strength $f_{sy} = 295.0$ MPa, ultimate tensile strength $f_{su} = 430.0$ MPa. The ratio of ultimate strength over yield strength is equal to 1.46, fulfilling the ductility requirements specified in both Eurocode 3 [28] and Chinese code GB 50017 [29]. Self-compacting concrete (SCC) that required little or no vibration effort was adopted to infill the steel tubes. The SCC was designed to achieve a nominal compressive cube strength at 28 days of 40 MPa by following JGJ/T 283 [30]. Based on the measured moisture content of sand, the mix proportions of the SCC were as follows: water, 154 kg/m³; cement, 443 kg/m³; sand, 782 kg/m³; coarse aggregate, 864 kg/m³; mineral admixture (coal fly ash), 111 kg/m³; water-reducing agent, 5.5 kg/m³. Nine standard cube tests on specimens of size 150 mm × 150 mm × 150 mm were conducted, and the average strength at the time of column testing was found to be 47.5 MPa.

The 17 test specimens under concentric compression (denoted as Group A, B and C) are listed in Table 1, and the other 17 test specimens under eccentric compression (denoted as Group D, E, F, G, H) are presented in Table 2. The test specimens were designed to cover a wide

**Table 1**
Details of test specimens under concentric compression.

| Specimen | $L$ (mm) | $L_e$ (mm) | $\lambda$ | $\beta$ | $\beta_a$ | $N_{u,Exp}$ (kN) |
|---|---|---|---|---|---|---|
| A0 (no infill) | 636 | 996 | 18.2 | 0 | 0 | 620 |
| A1 | 636 | 996 | 25.1 | 0 | 0 | 1450 |
| A2 | 636 | 996 | 25.1 | 0.2 | 0.21 | 1385 |
| A3 | 636 | 996 | 25.1 | 0.4 | 0.41 | 1340 |
| A4 | 636 | 996 | 25.1 | 0.6 | 0.62 | 1425 |
| A5 | 636 | 696 | 17.5 | 0.8 | 0.81 | 1331 |
| B1 | 1590 | 1950 | 49.1 | 0 | 0 | 1305 |
| B2 | 1590 | 1950 | 49.1 | 0.2 | 0.22 | 1133 |
| B3 | 1590 | 1950 | 49.1 | 0.4 | 0.45 | 945 |
| B4 | 1590 | 1950 | 49.1 | 0.6 | 0.67 | 1254 |
| B5 | 1590 | 1650 | 41.5 | 0.8 | 0.87 | 971 |
| C0 (no infill) | 2544 | 2904 | 53.0 | 0 | 0 | 474 |
| C1 | 2544 | 2904 | 73.1 | 0 | 0 | 1198 |
| C2 | 2544 | 2904 | 73.1 | 0.2 | 0.25 | 1130 |
| C3 | 2544 | 2904 | 73.1 | 0.4 | 0.49 | 1140 |
| C4 | 2544 | 2904 | 73.1 | 0.6 | 0.74 | 1020 |
| C5 | 2544 | 2904 | 73.1 | 0.8 | 0.99 | 948 |

range of key parameters, including the effective length ($L_e$), the initial stress ratio ($\beta$) and the load eccentricity ratio ($e/r$). Among which two test specimens - A0 and C0, not strengthened by infilling concrete, were used to quantify the strengthening effect. The effective length of the columns was taken as the geometric length ($L$) plus the lengths of the two pinned ends, dependent on the experimental devices for implementation of preload. The definitions of the slenderness ratio ($\lambda$), the initial stress ratio ($\beta$) and the preload ratio ($\beta_a$) are as follows,

$$\lambda = \frac{4L_e}{D} \quad (1)$$

$$\beta = \frac{N_P}{N_{sy}} = \frac{\sigma_0}{f_{sy}} \quad (2)$$

$$\beta_a = \frac{N_P}{N_{bc}} = \frac{\sigma_0}{\varphi f_{sy}} \quad (3)$$

where $N_{sy}$ is the cross-sectional plastic resistance of the steel column, and $N_{bc} = \varphi A_s f_{sy}$ is the overall buckling capacity of the steel column, $\varphi$ is the overall stability coefficient of the steel tubes according to the design provisions in Chinese design code for steel structures - GB 50017 [29] which can be determined from the relevant buckling curve, $\sigma_0 = N_P/A_s$ is the initial stress generated by the preload $N_P$, $A_s$ and $f_{sy}$ are the cross-sectional area and measured yield strength of the steel tube, respectively.

**Table 2**
Details of test specimens under eccentric compression.

| Specimen | $L$ (mm) | $L_e$ (mm) | $\lambda$ | $\beta$ | $\beta_a$ | $e$ (mm) | $e/r$ | $N_{u,Exp}$ (kN) |
|---|---|---|---|---|---|---|---|---|
| D1 | 636 | 996 | 25.1 | 0.6 | 0.62 | 30 | 0.38 | 910 |
| D2 | 1113 | 1473 | 37.1 | 0.6 | 0.64 | 30 | 0.38 | 890 |
| D3 | 1590 | 1950 | 49.1 | 0.6 | 0.67 | 30 | 0.38 | 690 |
| D4 | 2067 | 2427 | 61.1 | 0.6 | 0.70 | 30 | 0.38 | 670 |
| D5 | 2544 | 2904 | 73.1 | 0.6 | 0.74 | 30 | 0.38 | 620 |
| E1 | 636 | 996 | 25.1 | 0.6 | 0.62 | 15 | 0.19 | 1135 |
| E2 | 636 | 696 | 17.5 | 0.6 | 0.61 | 45 | 0.57 | 648 |
| F1 | 636 | 996 | 25.1 | 0 | 0 | 30 | 0.38 | 1010 |
| F2 | 636 | 996 | 25.1 | 0.2 | 0.21 | 30 | 0.38 | 990 |
| F3 | 636 | 996 | 25.1 | 0.4 | 0.41 | 30 | 0.38 | 950 |
| F4 | 636 | 996 | 25.1 | 0.8 | 0.83 | 30 | 0.38 | 835 |
| G1 | 2544 | 2904 | 73.1 | 0.6 | 0.74 | 15 | 0.19 | 710 |
| G2 | 2544 | 2604 | 65.5 | 0.6 | 0.71 | 45 | 0.57 | 486 |
| H1 | 2544 | 2904 | 73.1 | 0 | 0 | 30 | 0.38 | 750 |
| H2 | 2544 | 2904 | 73.1 | 0.2 | 0.25 | 30 | 0.38 | 665 |
| H3 | 2544 | 2904 | 73.1 | 0.4 | 0.49 | 30 | 0.38 | 600 |
| H4 | 2544 | 2604 | 65.5 | 0.8 | 0.95 | 30 | 0.38 | 608 |

## 2.2. Test setup and instrumentation programme

The working loads pre-applied on the steel columns were produced by means of two different experimental devices in this study. For the test specimens with initial stress ratio ($\beta$) higher than 0.6 or load eccentricity >30 mm, two mechanical jacks with load cells were utilised to deliver the designed preload directly, as shown in Fig. 1 (a). Two adjustable knife edges were introduced at the column ends, and the load eccentricity was achieved by moving the ridge to the corresponding V-shaped groove far away as the eccentricity distance from the column center. By means of this experimental device, preloads for five test specimens including A5, B5, E2, G2 and H4 were successfully applied. The second experimental device involved four pre-stressing screw bars and was employed for all the remaining test specimens, as show in Fig. 1 (b), where two rigid cover plates that provided reliable anchorage to the screw bars were attached to the column ends. A total of eight strain gauges were attached to the screw bars and used herein to monitor the preload level and corresponding load eccentricity. In general, a slightly greater preload was applied and monitored for one week with appropriate consideration of the possible stress relaxation of the screw bars. Once the preload level and load eccentricity stabilised, the SCC was filled and placed to air-dry until testing, typically 28 days later at least.

Since the components in the two support devices were different, it should be noted that the end length for the first experimental device was determined as 2 × 30 mm, while the corresponding end length for the second device were 2 × 180 mm owing to the thick end cover plates. The effective lengths of the test specimens were therefore obtained by adding the two end lengths to the measured steel tube length, as presented in Tables 1 and 2.

The overall buckling tests were carried out by using a 5000 kN capacity hydraulic testing machine, as shown in Fig. 1. The pin-ended boundary conditions were achieved by means of knife edges at both ends. For the concentrically loaded test specimens, the geometrical centering was implemented by putting the ridge of the knife edge into the central V-shaped groove, while the designed eccentricity for the eccentrically loaded test specimens was obtained by adjusting the ridge to the prescribed groove. There were a total of three digital linearly-varying displacement transducers (LVDTs) and eight strain gauges set up for each specimen, as illustrated in Fig. 1. Specifically, two LVDTs were used to determine the end-shortenings, and the third LVDT measured the mid-height lateral deflections; all the eight strain gauges were used to monitor the longitudinal and transverse strains at mid-height.

## 2.3. Loading tests and analysis of test results

Testing was conducted in load control. Specifically, a load interval of 5% of the estimated load capacity was applied until the extreme fibre of the steel tube reached material yielding, and then it was reduced to 2% of the estimated load capacity. Each load interval was maintained for 2 min or until the load stabilised, and the corresponding deformation and strain readings were recorded. During testing, the increasing axial load was accompanied by a gradual reduction of tension forces in the threaded rods (Fig. 1(b)). Once the rod tension forces reduced to zero, the rods were removed from the rigid end cover plates. For the five test specimens that were preloaded by two mechanical jacks, the corresponding load cells could be used to monitor load transfer from the mechanical jacks to the hydraulic jack. The mechanical jacks were also removed when the monitored loads approached zero. The experiment was terminated when the load reached or was less than the peak load in the descending path. The descending branch was thereby obtained through a controlled release of the hydraulic pressure.

All 34 test specimens exhibited overall flexural buckling as the primary failure mode, and the residual deformed shapes of tested columns with various column slenderness ratios are presented in Fig. 2. The residual deformed shapes correspond to sinusoidal waveforms between the two pinned ends. After peak load, local buckling of the steel tubes was observed at the compression side at approximately mid-height.

The experimental load versus axial end shortening curves were measured for the concentrically loaded columns (Group A, B and C), while the experimental load versus lateral deflection curves were obtained for the tested columns under eccentric compression. The two types of experimental curves are plotted in Figs. 3 and 4, respectively. It can be noted that all the specimens under eccentric compression and the majority of the concentrically loaded columns failed with a
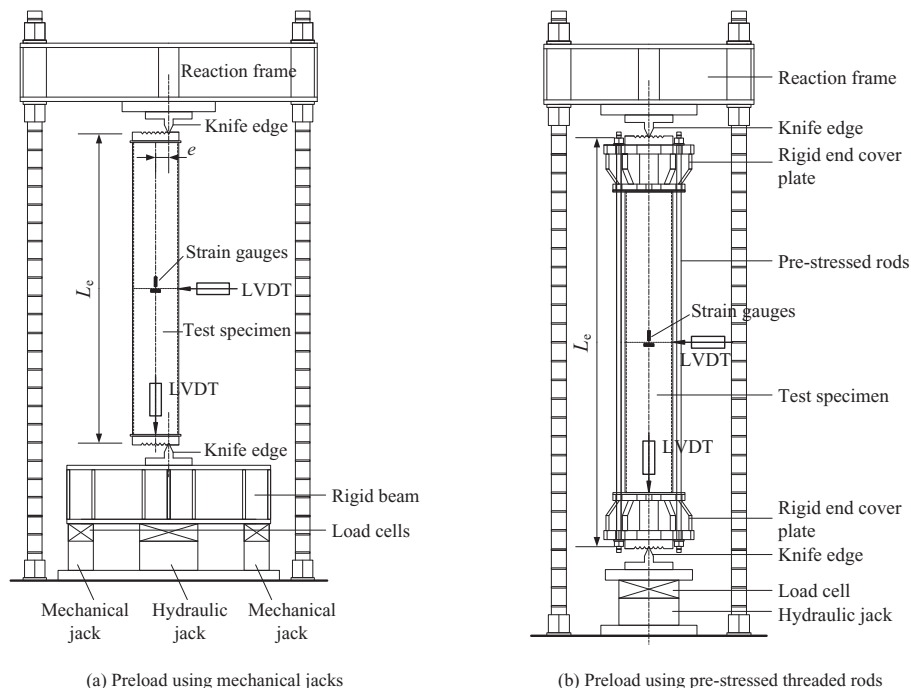


(a) Preload using mechanical jacks

(b) Preload using pre-stressed threaded rods

**Fig. 1.** Test setup and instrumentation programme.

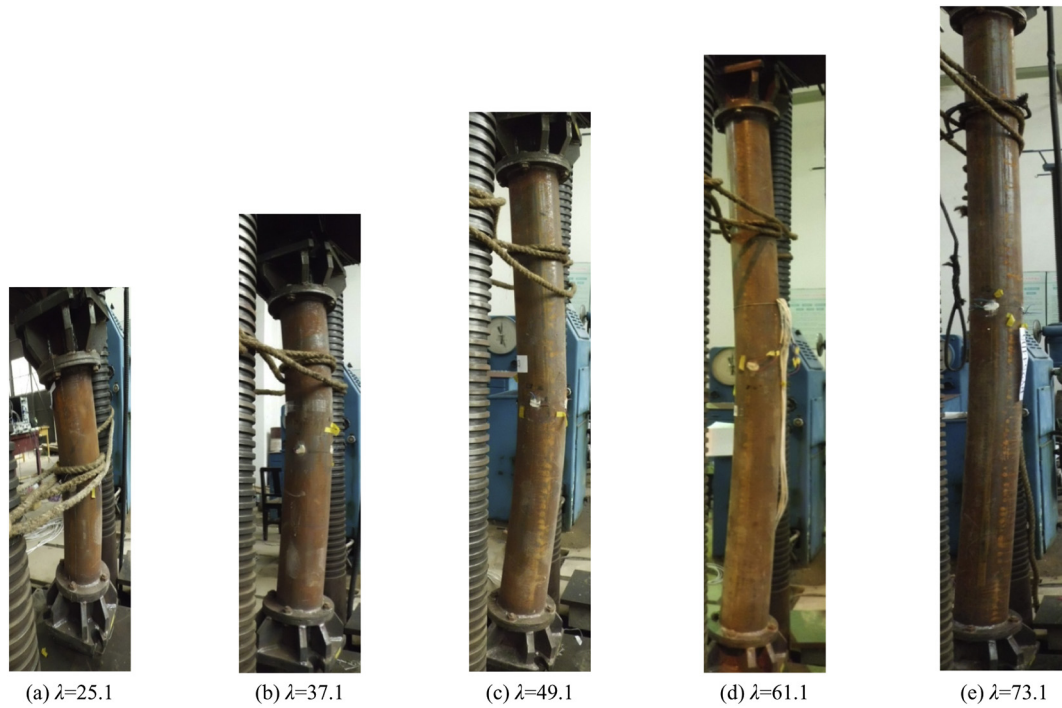(a) λ=25.1          (b) λ=37.1          (c) λ=49.1          (d) λ=61.1          (e) λ=73.1

**Fig. 2.** Residual deformed shapes of tested specimens with various column slenderness ratios.

ductile behaviour, while Group A test specimens underwent sudden buckling collapse, as illustrated in Figs. 3 and 4.

The measured ultimate load-carrying capacities of the test specimens are listed in Tables 1 and 2, and are also provided in Figs. 5–7. The significant strengthening effect from infilling concrete for CHS columns is verified by comparing specimens - A0 and A1, C0 and C1, resulting in 134% and 153% increase in compressive strength, respectively. Therefore, the ultimate load-carrying capacities for both concentrically and eccentrically loaded test specimens were reduced due to the presence of preload, especially for the tested columns with higher initial stress ratios. A decrease of nearly 10% in ultimate strength for the short columns (λ = 25.1) was observed, while the strength reduction was found to be about 25% for intermediate and slender columns. The ultimate load-carrying capacities were further reduced by increasing either the slenderness ratio or the load eccentricity, as illustrated in Figs. 6 and 7. Nevertheless, it can be noted that there are certain test specimens, such as A4 and B4, exhibiting abnormally higher experimental strength values, which may be attributed to the possible strength variations in concrete infill.

## 3. Numerical modelling

### 3.1. Numerical models

The numerical models for the CHS columns strengthened by infilling concrete were developed by means of the general finite element (FE) software package ABAQUS [31]. The general purpose 4-node shell element S4R was used to mesh the steel tube, and the continuum 8-node solid element C3D8R was adopted to mesh the infilled concrete core. Using the reduced integration method, both elements usually result in lower computational costs without undermining the accuracy of strain and stress results. The default total stiffness approach available in ABAQUS/Standard was adopted as the hourglass control approach. The number of section points throughout the shell thickness was set as nine for S4R elements by using the Simpson's integration rule. By means of the structured meshing technique, predefined mesh patterns were generated by dividing the circle into 32 elements (see Fig. 8), and the longitudinal element size was then determined by considering consistent element aspect ratios. Further mesh convergence studies
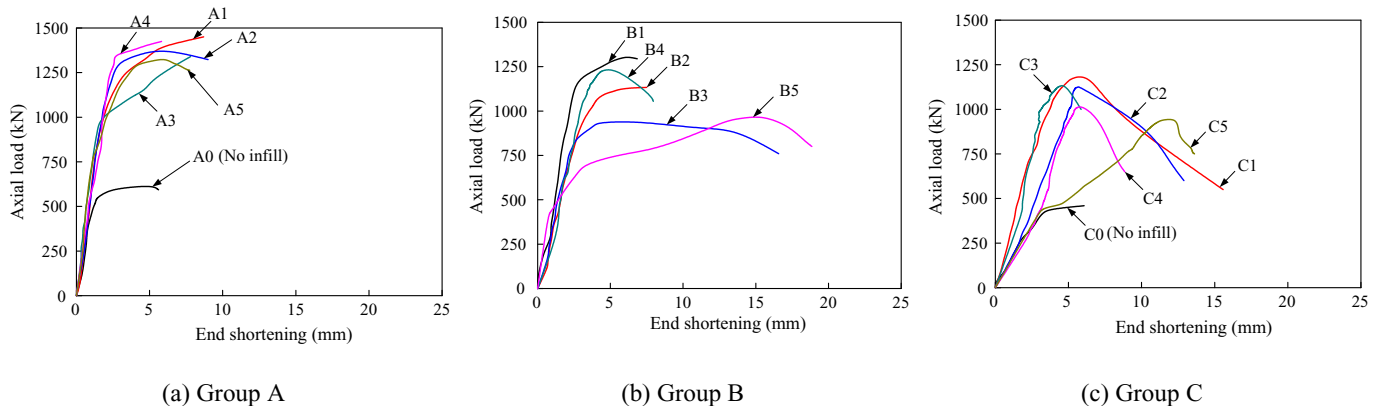


(a) Group A          (b) Group B          (c) Group C

**Fig. 3.** Axial load versus end shortening curves for the Group A, B and C test specimens under concentric compression.

(a) Group D
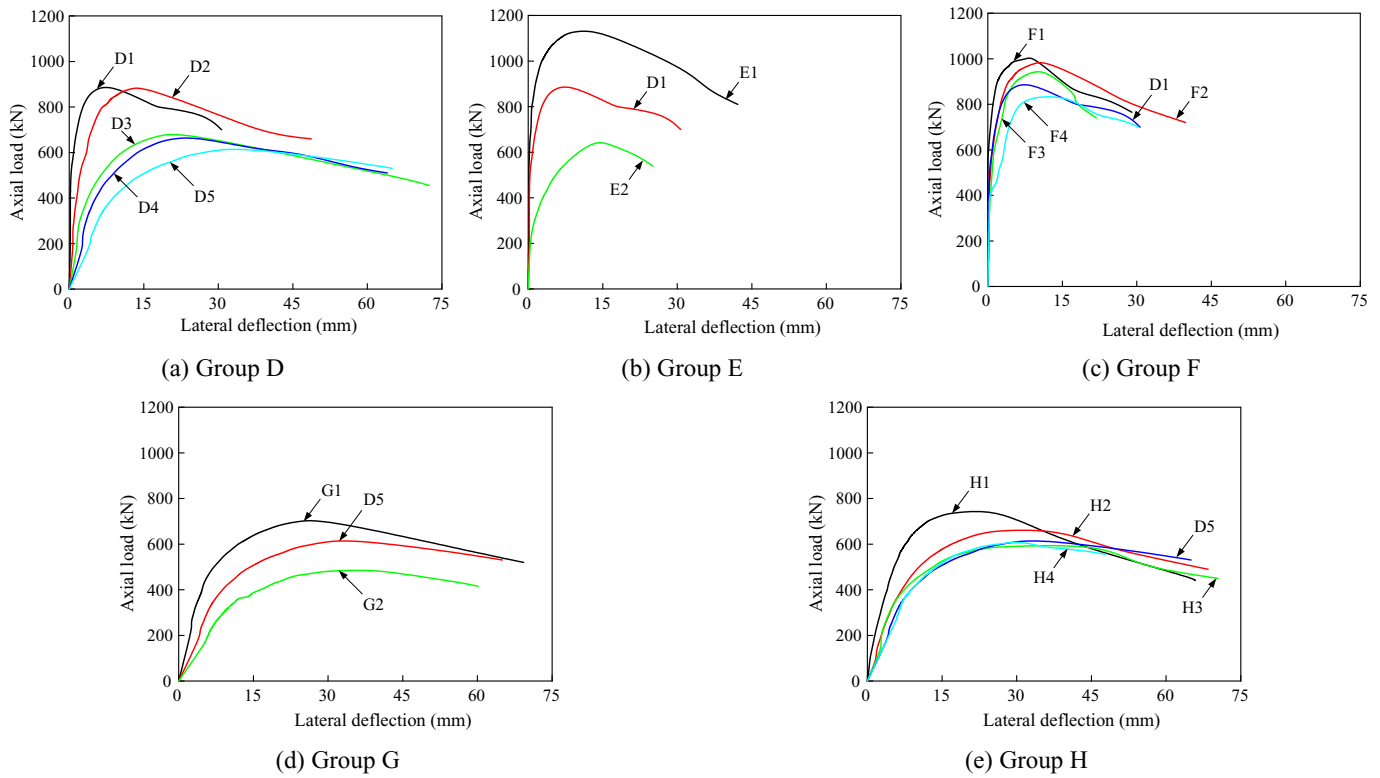
(b) Group E

(c) Group F

(d) Group G

(e) Group H

**Fig. 4.** Axial load versus lateral deflection curves for the Group D, E, F, G and H test specimens under eccentric compression.

were carried out to achieve satisfactory balance between computational time and accuracy of solution. The generated mesh for a typical test specimen B1 contained approximately 10,000 elements. It was revealed that, by introducing a much finer mesh with four times the number of elements, no >0.5% improvement in accuracy was obtained.

The material properties of the steel tube and the infilled concrete were considered by using the constitutive models proposed by Ding et al. [32], as illustrated in Fig. 9, which were also successfully applied in previous numerical studies [33,34]. Though the local buckling of steel tubes was observed in the post-ultimate stage for some test specimens, the finite slip between pairs of surfaces appeared to have negligible influence on the ultimate load-carrying capacity. Due to the fact that relative slip was not observed at the interface of steel and concrete before reaching the ultimate resistance, perfect bond between steel tube and infilled concrete was assumed and employed in the numerical models.

Initial global geometric imperfections of the test specimens were not experimentally measured in this study, an amplitude of 1/1000 of the column length, according to the GB 50205 [35], was assumed. It is widely recognised that the effects of initial global imperfections need to be incorporated within the analysis, the sensitivity of which will be discussed later. A linear eigenvalue buckling analysis was carried out to generate the global imperfection pattern, which were applied in the numerical models by means of the ABAQUS *IMPERFECTION command. Due to the relatively small outer diameter over wall thickness ratio of the steel tubes, local buckling of steel tube was not observed prior to overall member buckling, as indicated in the tests, and thus initial local geometric imperfections were not included. Moreover, the influence of welding residual stresses was not taken into account due to its negligible effect on ultimate buckling resistance, which here is primarily attributed to the introduction of concrete infill, per Tao et al. [36,37]. The pin-ended boundary conditions of the tests were replicated in the
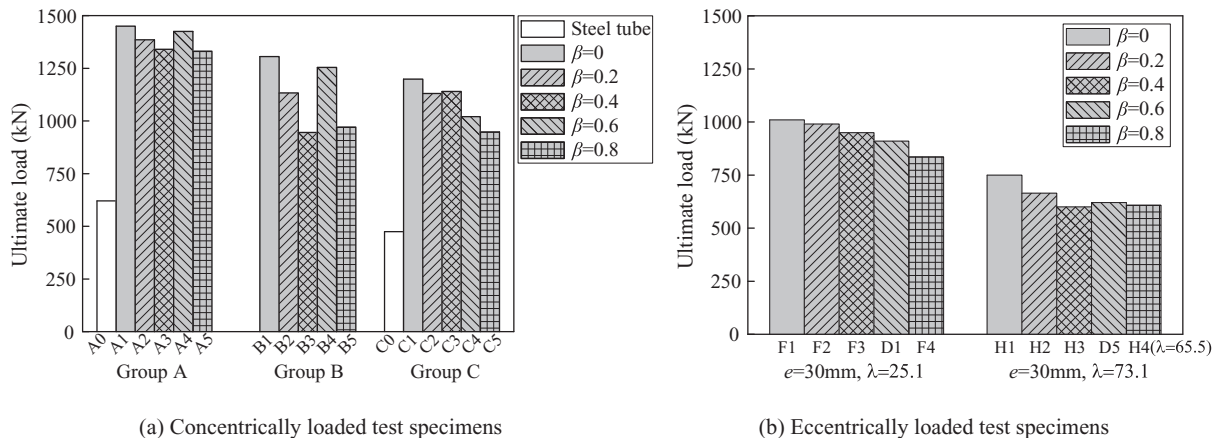


(a) Concentrically loaded test specimens

(b) Eccentrically loaded test specimens

**Fig. 5.** Comparison of ultimate load-carrying capacities for the test specimens with various initial stress ratios.
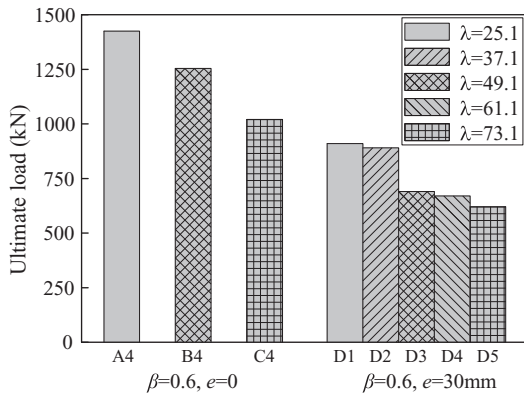
**Fig. 6.** Comparison of ultimate load-carrying capacities for the tested specimens with various slenderness ratios.

numerical models. All degrees of freedom were fixed except for the rotation about the in-plane axis at the upper end, while four degrees of freedom were fixed at the bottom end, allowing for the same rotation and longitudinal displacement.

There were two steps utilised to implement the preload and subsequent loading process:

(1) Applying the preload to the steel tube. The ABAQUS *MODEL CHANGE, REMOVE command was used to simulate the hollow steel tube by removing the concrete core. Herein the designed preload was applied on the steel tube with no further element calculations performed for the concrete core.

(2) Analysis of the steel tube strengthened by infilling concrete. The previously removed concrete core was reactivated by using the ABAQUS *MODEL CHANGE, ADD command. The subsequent loading process was achieved by applying the longitudinal displacement at the bottom end, thus the imposed loads could be undertaken by both the steel tube and infilled concrete. The geometric nonlinearity was explicitly considered throughout the analysis.

### 3.2. Validation of the FE models

The numerical modelling results were compared with the obtained test data. A comparison between the experimental and numerical load versus deformation curves is given in Fig. 10, and the ultimate buckling resistances predicted by the FE models are compared with those obtained from the tests, as presented in Fig. 11 (a), where $N_{u, FE}$ and $N_{u, Exp}$ are the ultimate loads from the FE models and tests, respectively. The mean value of the $N_{u, FE}/N_{u, Exp}$ ratio is 1.01 with a corresponding coefficient of variation (COV) of 0.11, and the load versus deformation
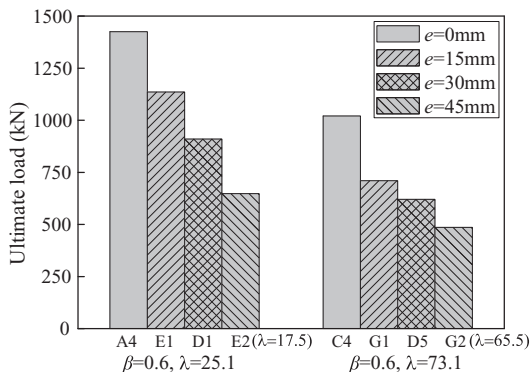


**Fig. 7.** Comparison of ultimate load-carrying capacities for the tested specimens with various eccentricities.
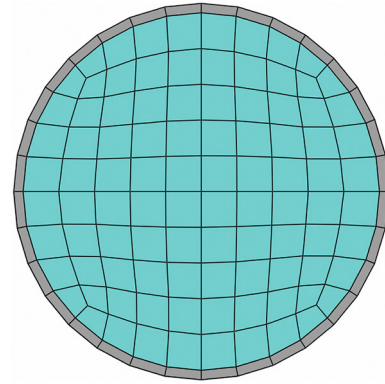


**Fig. 8.** Discretisation of the steel tube section with concrete infill.

curves reproduced by the FE models exhibit good agreement with the experimental curves.

Meanwhile, other available existing test data were summarised and used to further validate the developed FE models. Zha [20] tested a total of 27 concrete-filled CHS columns with various preload ratios, which were 133 mm × 4.5 mm steel tubes ($f_{sy}$ = 325 MPa) with infilled concrete ($f_{ck, cube}$ = 42.2 MPa). Huang and Chen [21] reported nine concrete-filled CHS column tests with initial stresses: the geometric dimension of the tested columns was 108 mm × 4 mm, the characteristic strengths for the steel tube and the infilled concrete were 336 MPa ($f_{sy}$) and 54.6 MPa ($f_{ck, cube}$), respectively. A total of 11 tests on concrete-filled composite columns subjected to preloads with steel tube of 219 mm × 6.3 mm were carried out by Liew and Xiong [22], where eight of which introduced the high strength concrete with $f_{ck} \geq 95$ MPa. The summarised 47 tests were therefore numerically modelled by means of the developed FE models, and the comparison of the FE predicted ultimate buckling resistances with the test data is shown in Fig. 11 (b) and (c). The mean value of $N_{u, FE}/N_{u, Exp}$ is 0.96 for test data from Zha [20] and Huang and Chen [21], and the corresponding COV value is 0.09, while the average $N_{u, FE}/N_{u, Exp}$ ratio is 0.92 with a COV of 0.11 for test data reported by Liew and Xiong [22], revealing slightly conservative and reliable estimation of ultimate buckling resistances of the tested columns. The underestimated ultimate strengths for the tested columns presented by Liew and Xiong [22] might be attributed to the fact that the previously employed constitutive model of concrete would not be able to cover the involved high strength concrete. It is therefore concluded that the FE models are capable of providing accurate predictions for the CHS columns strengthened by infilling concrete subjected to preload, enabling the following systematic numerical studies on the major parameters.

### 3.3. Parametric studies

Based upon the validated FE models, parametric studies were conducted herein. The influences of the major input parameters, including preload ratios, steel and concrete strengths, steel ratios, initial global imperfections, eccentricity ratios and column slenderness ratios were further explored. There were a total of 590 generated numerical models, which were facilitated by means of the ABAQUS *PARAMETRIC command. A preload reduction factor $k_\beta$, defined by Eq. (4), is introduced to assess the effect of preload on the ultimate buckling resistances, and it can be seen that a smaller value of the factor $k_\beta$ corresponds to more severe strength reduction due to preload.

$$k_\beta = \frac{N_{u,\beta}}{N_{u0}} \qquad (4)$$

where $N_{u, \beta}$ and $N_{u0}$ are the ultimate resistances from CHS steel columns strengthened by infilling concrete with and without preload, respectively.
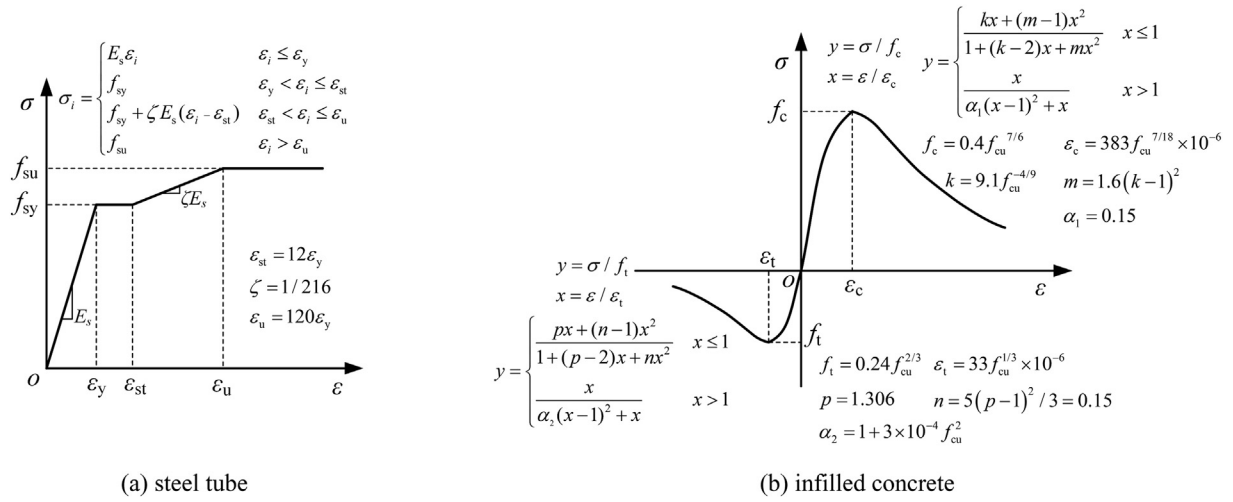
(a) steel tube

(b) infilled concrete

**Fig. 9.** The adopted constitutive models for the steel tube and the infilled concrete.



(a) A4

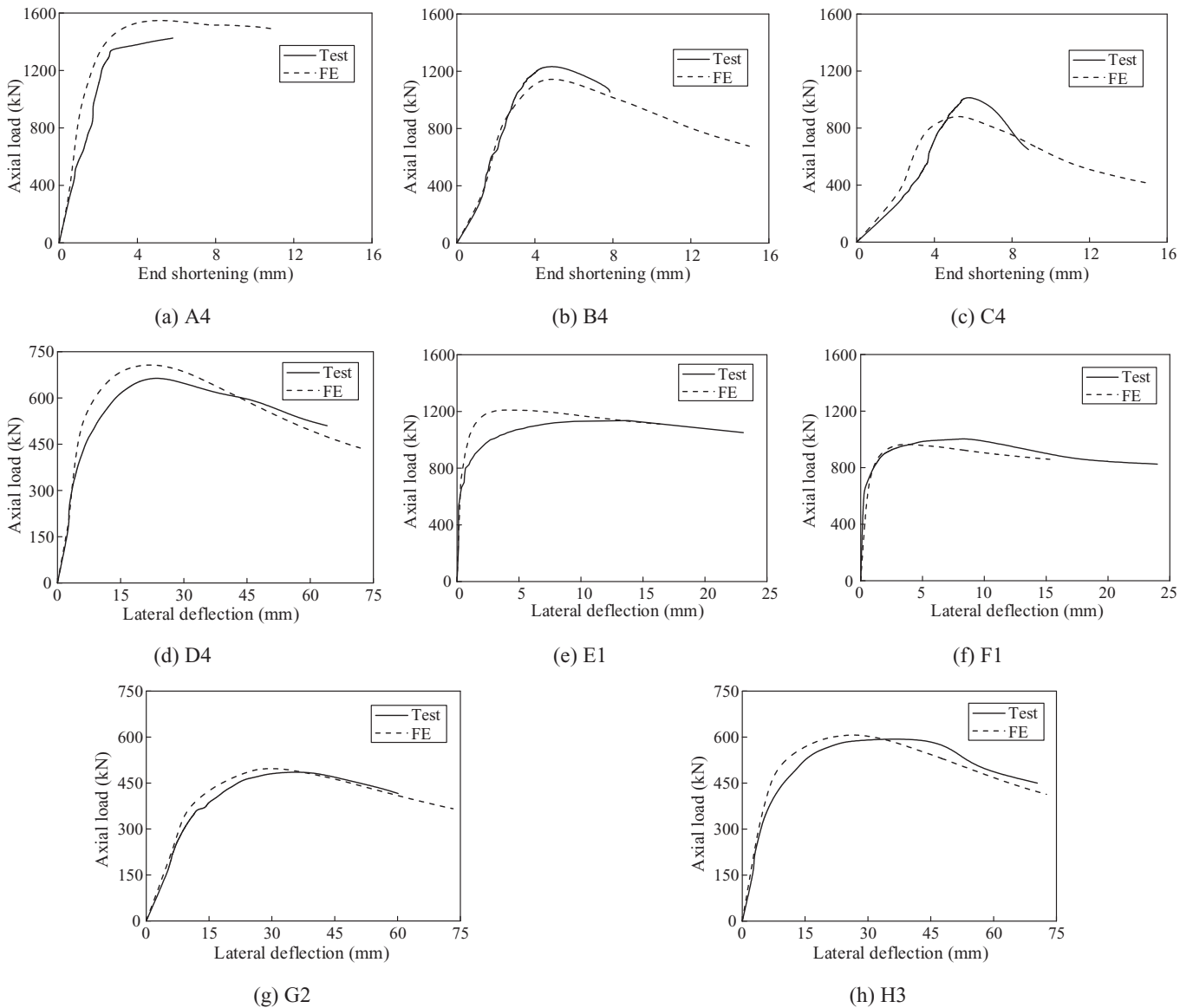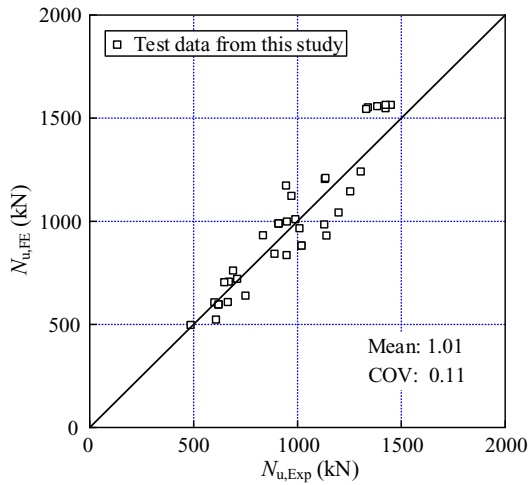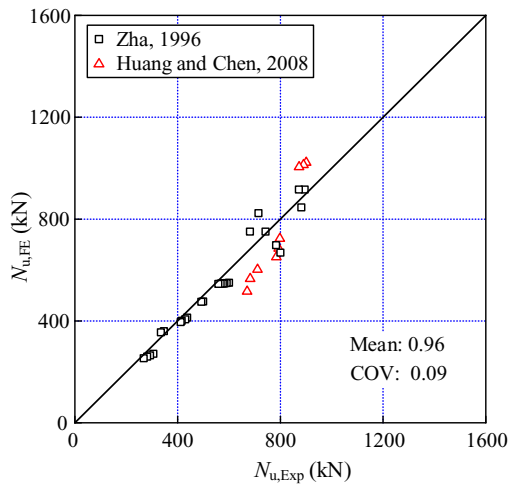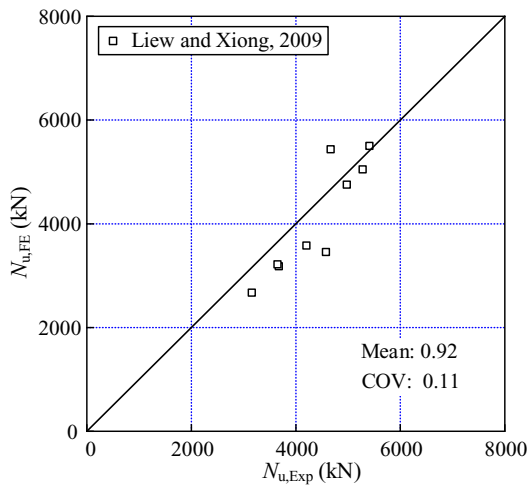(b) B4

(c) C4

(d) D4

(e) E1

(f) F1

(g) G2

(h) H3

**Fig. 10.** Comparison of load versus deformation curves between tests and FE modelling for typical specimens.

(a) Test results presented in this study



(b) Tests published by Zha [20] and Huang and Chen [21]



(c) Tests published by Liew and Xiong [22]

**Fig. 11.** Comparison of ultimate buckling resistances from FE predictions and summarised tests.

Three different steel grades and four types of concrete strength were chosen to investigate their possible impact on the ultimate load-carrying capacities. The numerical analysis on the steel and concrete strength effect was carried out separately, and the corresponding results are presented in Figs. 12 and 13. It is shown that increasing material strength of steel tubes leads to different consequences for columns with various slenderness ratios. Specifically, the strength reduction effect at a given preload ratio ($\beta_a$) is more evident for intermediate columns ($\lambda = 40$) with higher steel grade, while for slender columns ($\lambda = 120$), on the contrary, the strength reduction becomes less prominent for higher steel grade. Meanwhile, raising the concrete strength of intermediate columns ($\lambda = 40$) decreases the strength reduction effect, which may be due to the fact that the strengthened columns can benefit from the higher concrete strength due to the full exploitation of its compressive strength. This condition does not exist for columns with higher slenderness ratios ($\lambda = 80$), since the full exploitation of compressive strength of the concrete core may not be achieved. Moreover, the variation of the preload reduction factor caused by the changes of concrete strength appears to be smaller than that resulted from different steel grades, thus it can then be approximated by considering the steel grade rather than the concrete strength in calculating the preload reduction effect.

The steel ratio $\alpha$ can be given as $\alpha = A_s/A_c$, where $A_s$ and $A_c$ are the cross-sectional area of the steel tube and the infilled concrete core, respectively. The influence of the steel ratio $\alpha$ was also examined by numerical modelling in this sub-section. Fig. 14 presents the comparison of the preload reduction factors involving a total of five different values of the steel ratio ranging from 0.050 to 0.200. It can be noticed that the preload reduction factor $k_\beta$ decreases when the steel ratio values for intermediate columns ($\lambda = 40$) is increased, especially in the case of columns with preload ratio beyond 0.5. This can be explained that raising initial preload ratio for the columns with higher steel ratio value indicates greater initial stresses in the steel tube, which may undermine its contribution to the overall buckling capacity of the columns, since the compressive strength of the infilled concrete core can be thoroughly exploited. While for the long and slender columns, the contribution from the concrete core to the overall buckling capacity of the columns may be reduced due to the limitation of much lower tensile strength of concrete, and an increase in buckling resistance is possible with higher values of the steel ratio, implying less prominent preload reduction effect. It can therefore be concluded that the influence of the steel ratio is generally small, especially for the columns with relatively lower preload ratios (≤0.5).

Four different amplitudes of the initial global imperfection (also referred to as initial curvature) - $L/500$, $L/1000$, $L/1500$ and $L/2000$, were considered in the numerical models. The possible influence of the initial global imperfection on the preload reduction effect is presented Fig. 15, and it is shown that increasing initial curvature has little effect on the preload reduction factor for both intermediate columns ($\lambda = 40$) and slender columns ($\lambda = 120$). While for long columns ($\lambda = 80$), the variation of initial curvature from $L/1000$ to $L/500$ results in higher values of preload reduction factor, especially for the columns with larger preload ratios. This can be explained that the tension region in cross-section of long columns generated by the relatively large global curvature increased with the preload ratio, thus reducing the influence of the preload. Moreover, the initial global imperfection amplitudes of steel columns are required to meet the tolerance of $L/1000$ given by the GB 50205 provisions [35], which is also widely accepted as a representative limit value [38]. Consequently, it would be considered to be unnecessary to take into account the initial geometric imperfection for determining the preload reduction factor, despite the fact that incorporating the initial geometric imperfections is essential to the development of design method to predict column buckling resistance in general [39,40].

The influence of the eccentricity ratio ($e/r$) was studied for the columns strengthened by infilling concrete, as presented in Fig. 16. It can be seen that the preload reduction factor increased with the eccentricity ratios, revealing less affect due to the initial stresses. Along with the increased eccentricity ratios, the tension zone of the infilled concrete would spread to cover the entire concrete core, which undermined
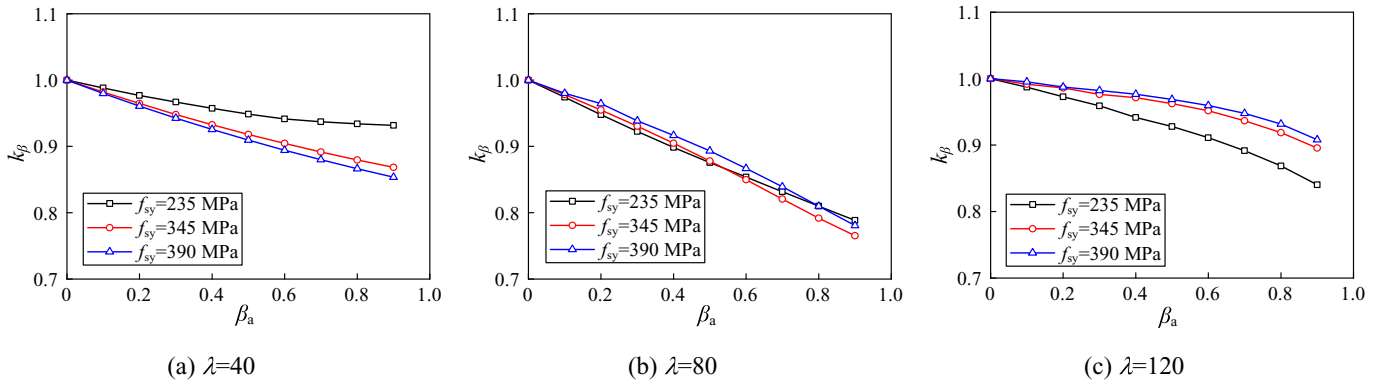
**Fig. 12.** Influence of yield strength of steel tube ($f_{ck, cube} = 40$ MPa, $\alpha = 0.1$, $e/r = 0$, $w = L/1000$).

the contribution of the infilled concrete due to the relatively lower tensile strength compared to its compressive strength. Moreover, for a given level of preload ratio (such as $\beta_a = 0.4$), the presence of preload can increase the axial force of the column, which may reduce the equivalent eccentricity value by comparing the existing bending moment to the total axial force, especially for those columns with higher eccentricity ratios. Hence, less reduction effect can be observed for the columns subjected to eccentric loading, and the obtained results herein agree well with those obtained by Han and Yao [19].

Furthermore, the numerical models were developed to cover a total of seven column slenderness ratios ranging from 10 to 120. The comparison of the preload reduction factor $k_\beta$ is plotted in Fig. 17 for two types of steel grades. It is indicated that the $k_\beta$ value decreases with increase of slenderness ratios for short and intermediate columns, and then a

reversed pattern is observed for columns with larger slenderness ratios, reflecting smaller influences from the preload. The critical slenderness ratios can be further determined by the three dimensional diagrams presented in Fig. 18. Specifically, the critical slenderness ratio for steel grade $f_{sy} = 235$ MPa approximates to 90, and the corresponding critical value for steel grade $f_{sy} = 345$ MPa can be taken as 80. In view of the similarity between steel grades of $f_{sy} = 345$ MPa and $f_{sy} = 390$ MPa as indicated in Fig. 12, the critical slenderness ratio for steel grade $f_{sy} = 345$ MPa can also be extended to cover the steel grade $f_{sy} = 390$ MPa.

## 4. Proposed design method

Based upon the parametric studies described above, the preload ratio, the steel grade, the eccentricity ratio and the column slenderness
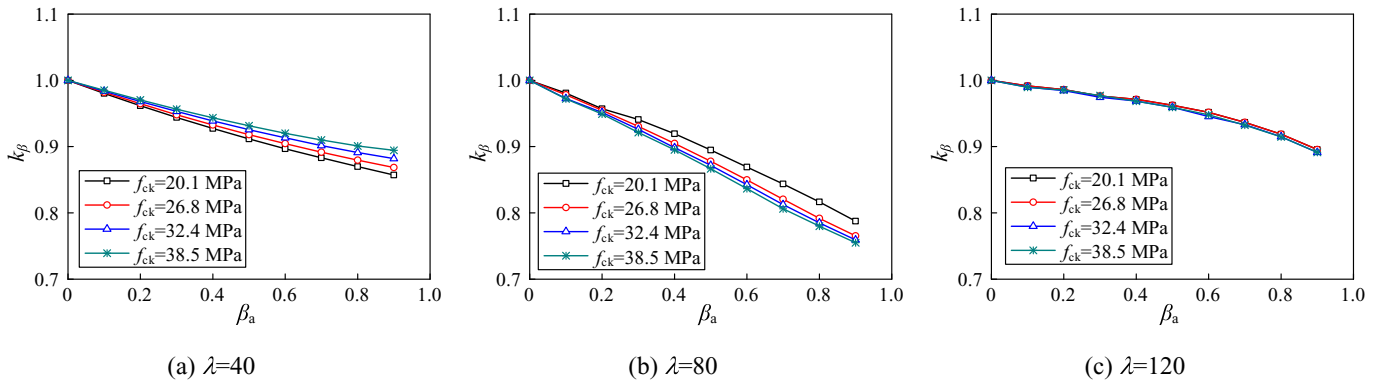


**Fig. 13.** Influence of infilled concrete strength ($f_{sy} = 345$ MPa, $\alpha = 0.1$, $e/r = 0$, $w = L/1000$).
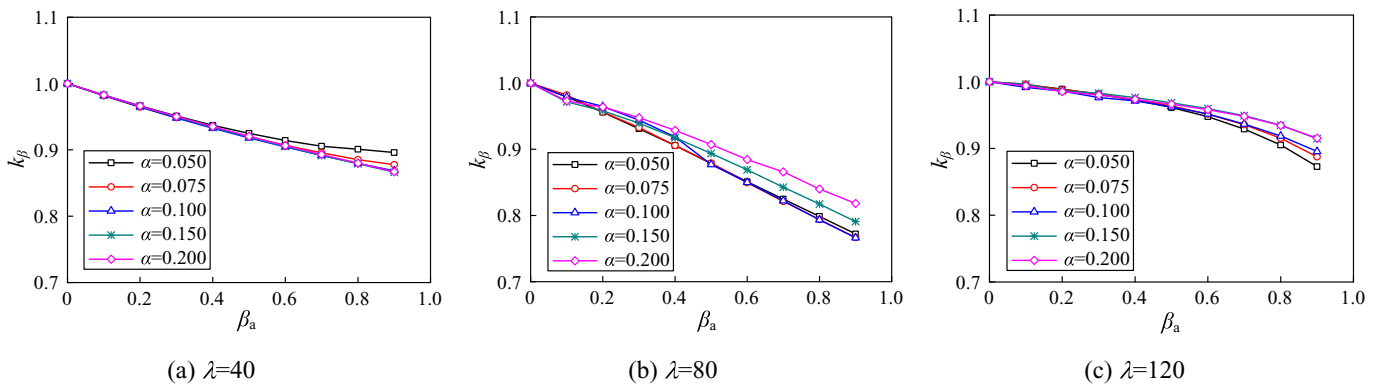


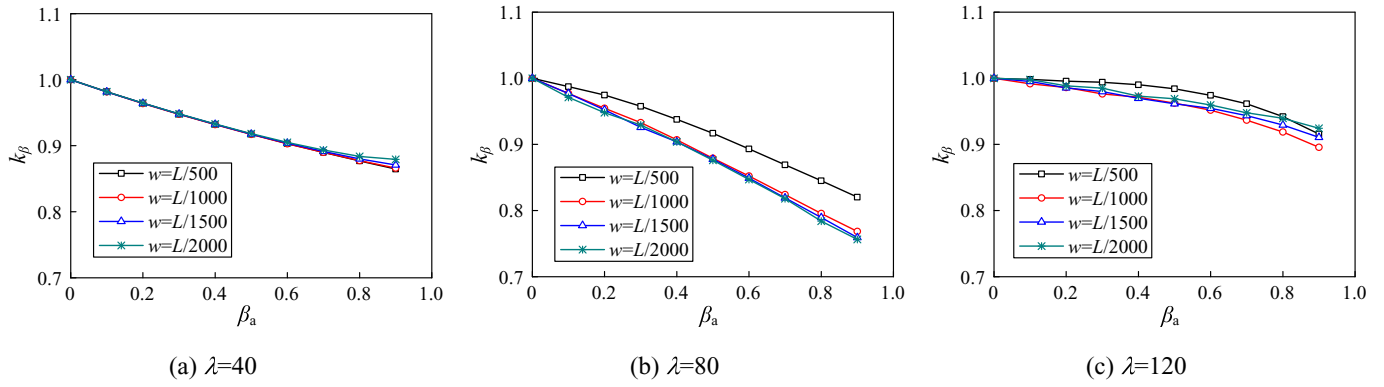**Fig. 14.** Influence of the steel ratio ($f_{sy} = 345$ MPa, $f_{ck, cube} = 40$ MPa, $e/r = 0$, $w = L/1000$).

**Fig. 15.** Influence of the initial curvature ($f_{sy} = 345$ MPa, $f_{ck, cube} = 40$ MPa, $\alpha = 0.1$, $e/r = 0$).
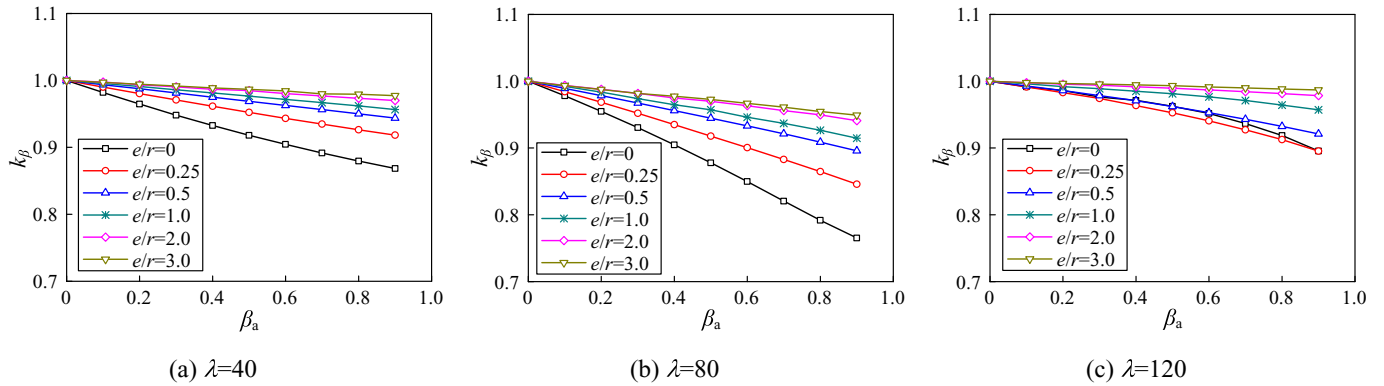


**Fig. 16.** Influence of the eccentricity ratio ($f_{sy} = 345$ MPa, $f_{ck, cube} = 40$ MPa, $\alpha = 0.1$, $w = L/1000$).

ratio have been demonstrated to be the key parameters which can have prominent effects on the overall buckling resistance of CHS steel columns strengthened by infilling concrete subjected to preload. Moreover, the generated numerical models incorporate a wide range of the major parameters – steel grade $f_{sy}$ (235 MPa, 345 MPa and 390 MPa), concrete strength $f_{ck}$ (20.1 MPa, 26.8 MPa, 32.4 MPa, 38.5 MPa), column slenderness ratio (10−120), steel ratio (0.05–0.20), eccentricity ratio $e/r$ (0–3.0) and global curvature ($L/2000$-$L/500$). These generated numerical data, along with the obtained test results, were used for developing design criteria for expected retrofit cases encountered in practice.

The ultimate resistances from CHS steel column strengthened by infilling concrete with preload ($N_{u,\beta}$) can be calculated by rewriting Eq. (4),

$$N_{u,\beta} = k_\beta N_{u0} \tag{5}$$

in which the ultimate resistance of CHS steel column strengthened by infilling concrete without preload ($N_{u0}$) is equivalent to that of the concrete-filled steel tubular column, and it can be determined by the design provisions provided in the Chinese technical code for concrete filled steel tubular structures (GB 50936) [41]. The ultimate resistance $N_{u0}$ is given as

$$N_{u0} = \varphi_e \varphi_l N_0 \tag{6}$$

where $\varphi_e$ and $\varphi_l$ are reduction factors that account for the eccentricity ratio and column slenderness ratio, respectively, $N_0$ is the cross-
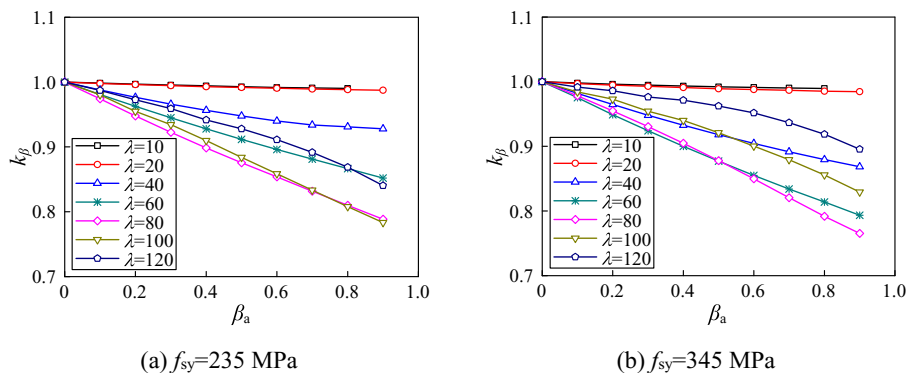


**Fig. 17.** Influence of the column slenderness ratio ($f_{ck, cube} = 40$ MPa, $\alpha = 0.1$, $e/r = 0$, $w = L/1000$).
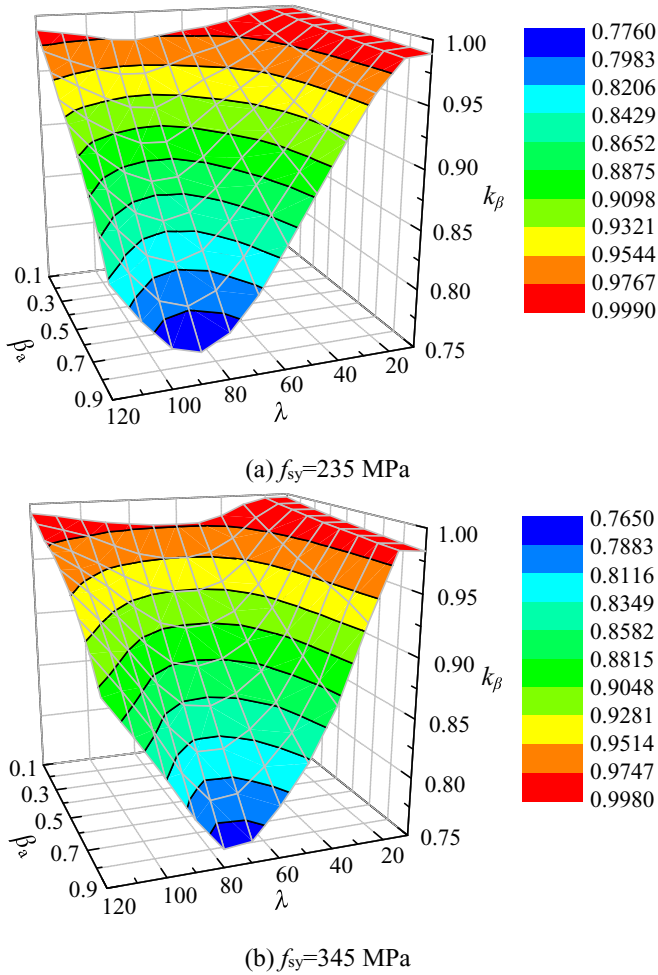
(a) $f_{sy}$=235 MPa



(b) $f_{sy}$=345 MPa

**Fig. 18.** Three dimensional diagrams involving the influence of column slenderness ratios ($f_{ck, cube} = 40$ MPa, $\alpha = 0.1$, $e/r = 0$, $w = L/1000$).

sectional resistance to concentric compression for stub columns, and may then be calculated from the following expression:

$$N_0 = \begin{cases} 0.9A_c f_c(1+\alpha_0\theta) & \theta \leq 1/(\alpha_0-1)^2 \\ 0.9A_c f_c\left(1+\sqrt{\theta}+\theta\right) & \theta > 1/(\alpha_0-1)^2 \end{cases} \quad (7)$$

where the confinement coefficient $\theta$ is defined as $\theta = A_s f_s/(A_c f_c)$, $A_s$ and $A_c$ are the cross-sectional area of the steel tube and the infilled concrete core, and $f_s$ and $f_c$ are the corresponding design strength of the steel and the concrete; $\alpha_0$ is another coefficient dependent on concrete strength, and can be taken as 1.8 for concrete with $f_{ck, cube}$ varying from 55 MPa to 80 MPa, and is equal to 2.0 for concrete with $f_{ck, cube} \leq 50$ MPa.

Meanwhile, the preload reduction factor $k_\beta$ can be determined as follows:

$$k_\beta = 1 - f(e/r)f(\lambda)\beta_a \quad (8)$$

in which $\beta_a$ is the preload ratio defined by Eq. (3), $f(e/r)$ is an eccentricity function provided in Eq. (9), $f(\lambda)$ is the basic column curve, and can be computed by Eqs. (10) and (11) for steel of $f_{sy} = 235$ MPa and $f_{sy} = 345$ MPa (390 MPa), respectively, where the previously acquired critical slenderness ratios are taken as the cross points of the piecewise functions.

$$f(e/r) = \frac{1}{1 + 1.871(e/r) - 0.029(e/r)^2} \quad (9)$$

$$f_{sy} = 235 \text{ MPa} \quad f(\lambda)$$
$$= \begin{cases} -0.032 + 0.289\frac{\lambda}{90} - 0.006\left(\frac{\lambda}{90}\right)^2 & \text{for } \lambda \leq 90 \\ -0.35 + 1.256\frac{\lambda}{90} - 0.655\left(\frac{\lambda}{90}\right)^2 & \text{for } \lambda > 90 \end{cases} \quad (10)$$

$$\begin{array}{c} f_{sy} = 345 \text{ MPa} \\ \left(f_{sy} = 390 \text{ MPa}\right) \end{array} \quad f(\lambda)$$
$$= \begin{cases} -0.060 + 0.553\frac{\lambda}{80} - 0.226\left(\frac{\lambda}{80}\right)^2 & \text{for } \lambda \leq 80 \\ 0.555 - 0.288\frac{\lambda}{80} & \text{for } \lambda > 80 \end{cases} \quad (11)$$

The calculated preload reduction factors ($k_{\beta, pre}$) were therefore compared with those derived by the numerical models ($k_{\beta, FE}$), as shown in Fig. 19. It can be seen from Fig. 19 that the majority of the data points lie within the region bounded by the +5% and −5% limit lines, and a close agreement is shown to exist between the calculated values and the numerical results.

The corresponding buckling resistances for the summarised tested columns with preload ($N_{u, \beta}$) can then be computed by $N_{u, \beta} = k_\beta N_{u0}$, and the comparison between the predicted buckling resistances and the summarised test results is plotted in Fig. 20. The mean value of predicted over test strength ratios is 0.96 with a corresponding COV of 0.10, indicating slightly conservative but sufficiently accurate strength predictions for design purposes. Therefore, the validity of the proposed design formulae has been verified by the experimental and numerical results.

Considering the inherent uncertainty during the strengthening process and the difficulty to determine the actual eccentricity ratio and other key parameters in practice, a new reduction coefficient $\eta_c$ was introduced herein to replace the preload reduction factor $k_\beta$. The numerically obtained data points of the preload reduction factor are presented in Fig. 21, and the values of the coefficient $\eta_c$ are proposed by referring to approximate lower envelope, as listed in Table 3 and plotted in Fig. 21. Thus a highly simplified and relatively conservative design approach has been obtained, which is also incorporated into the revision of the Chinese code for design of strengthening steel structures [27].

## 5. Conclusions

Comprehensive experimental and numerical studies on circular hollow section (CHS) steel columns retrofitted by infilling concrete have been carried out. A total of 34 CHS steel column specimens with various slenderness ratios subjected to preload were strengthened by concrete infill and were tested under pin-ended boundary conditions, failed by overall flexural buckling. The ultimate load-carrying capacities of the CHS columns strengthened by infilling concrete were obtained. Finite element (FE) models developed using ABAQUS were validated against the obtained test results and other available test data.

By means of the validated FE models, parametric studies were carried out to examine the major factors that can affect the ultimate capacity, generating a set of 590 strengthened CHS column models under preload. It is shown that the steel grade instead of concrete strength, the eccentricity ratio and the column slenderness ratio should be considered together with the preload ratio, while the influences of the steel ratio and the initial global geometric imperfection are relatively small. Based on the obtained test and numerical results, a newly developed design approach for predicting the overall buckling resistance of CHS columns strengthened by infilling concrete under preload was presented in the framework of Chinese code GB 50936, and the accuracy of the proposed design formulae was verified. Finally, a simplified reduction coefficient taking into the effect of the existing preload was introduced, in view of the inherent uncertainty of retrofitting and difficulty
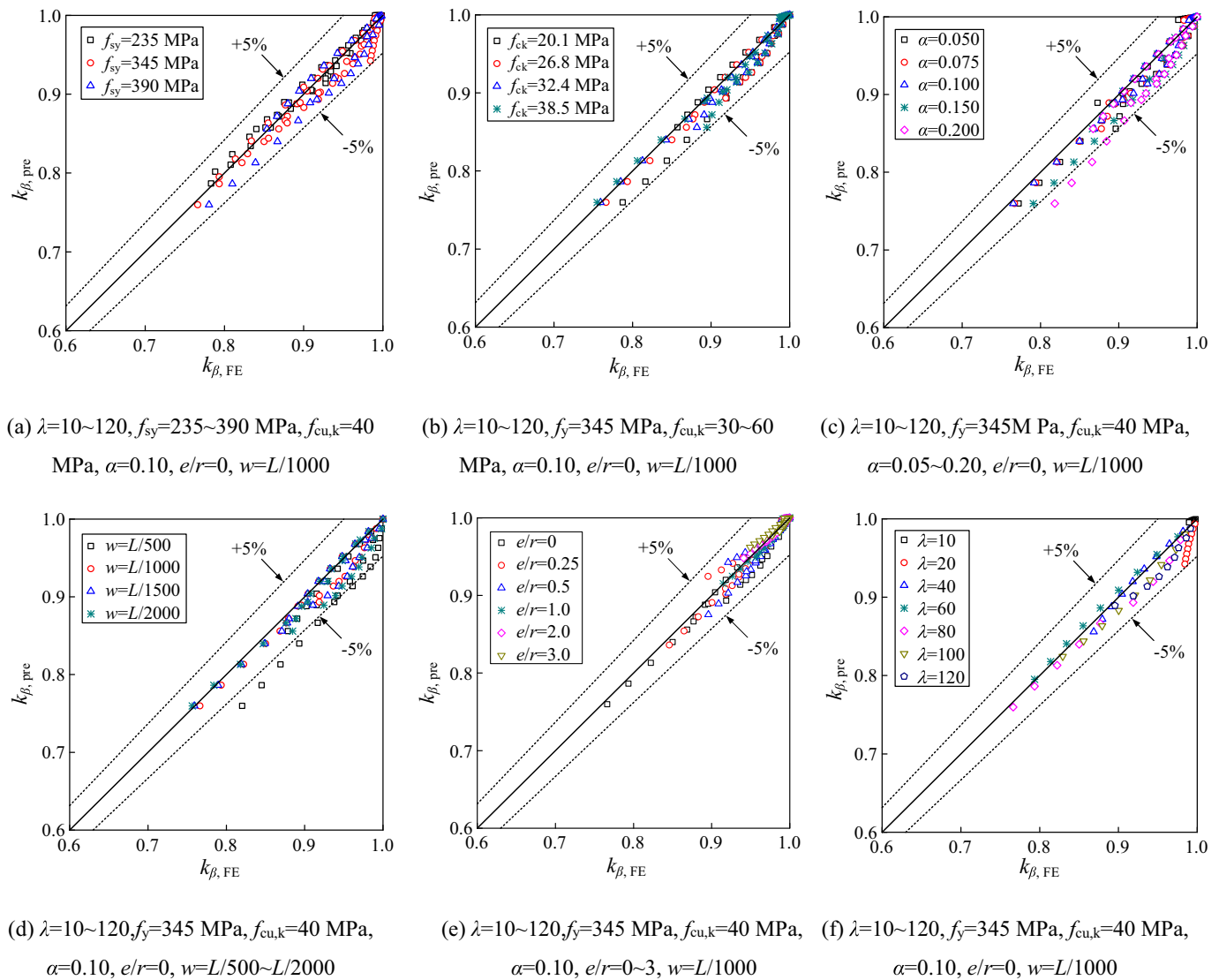
(a) $\lambda$=10~120, $f_{sy}$=235~390 MPa, $f_{cu,k}$=40 MPa, $\alpha$=0.10, $e/r$=0, $w$=$L$/1000

(b) $\lambda$=10~120, $f_y$=345 MPa, $f_{cu,k}$=30~60 MPa, $\alpha$=0.10, $e/r$=0, $w$=$L$/1000

(c) $\lambda$=10~120, $f_y$=345M Pa, $f_{cu,k}$=40 MPa, $\alpha$=0.05~0.20, $e/r$=0, $w$=$L$/1000

(d) $\lambda$=10~120, $f_y$=345 MPa, $f_{cu,k}$=40 MPa, $\alpha$=0.10, $e/r$=0, $w$=$L$/500~$L$/2000

(e) $\lambda$=10~120, $f_y$=345 MPa, $f_{cu,k}$=40 MPa, $\alpha$=0.10, $e/r$=0~3, $w$=$L$/1000

(f) $\lambda$=10~120, $f_y$=345 MPa, $f_{cu,k}$=40 MPa, $\alpha$=0.10, $e/r$=0, $w$=$L$/1000

**Fig. 19.** Comparison of preload reduction factors obtained from the proposed formulae and the numerical models.
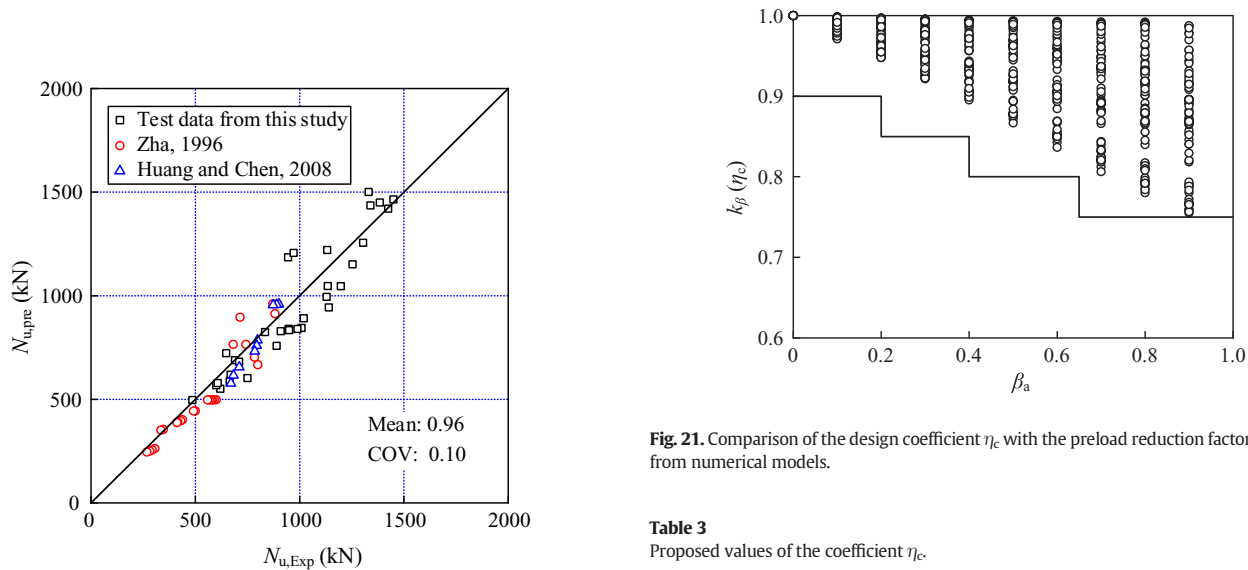


**Fig. 20.** Comparison between predicted buckling resistances from the proposed design method and summarised test results.
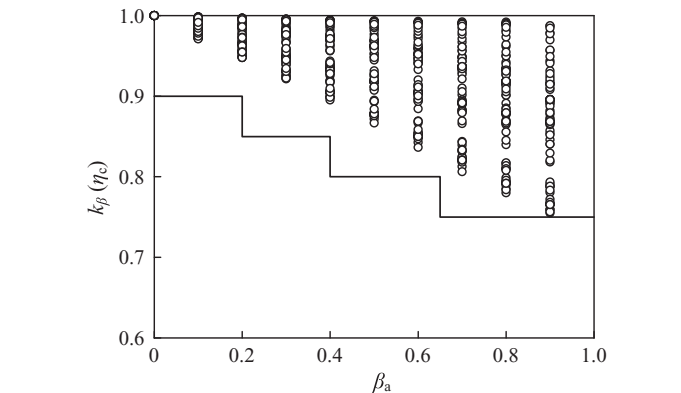


**Fig. 21.** Comparison of the design coefficient $\eta_c$ with the preload reduction factors derived from numerical models.

**Table 3**
Proposed values of the coefficient $\eta_c$.

| Preload ratio $\beta_a$ | $\beta_a \leq 0.2$ | $0.2 < \beta_a \leq 0.4$ | $0.4 < \beta_a \leq 0.65$ | $\beta_a > 0.65$ |
|---|---|---|---|---|
| Coefficient $\eta_c$ | 0.90 | 0.85 | 0.80 | 0.75 |

of determining the key parameters encountered in practice. The developed design guidance is expected to be used in retrofit cases for CHS steel columns, with further design checks to be conducted by including the increased self-weight from infilling concrete to the existing structural system.

## Acknowledgements

## References

[1] N.R. Nagaraja Rao, L. Tall, Columns reinforced under load, Weld. J. 42 (1963) Reprint No. 216 (63–2), Fritz Laboratory Report. Paper 144.

[2] L. Tall, The reinforcement of steel columns, AISC Eng. J. (1989) 33–37 1st Quarter.

[3] Y.Q. Wang, L. Zong, R.X. Zhu, X.Y. Liu, Y.J. Shi, Behavior of I-section steel beam welding reinforced while under load, J. Constr. Steel Res. 106 (2015) 278–288.

[4] A.K. Bhowmick, G.Y. Grondin, Limit state design of steel columns reinforced with welded steel plates, Eng. Struct. 114 (2016) 48–60.

[5] X.L. Zhao, L. Zhang, State-of-the-art review on FRP strengthened steel structures, Eng. Struct. 29 (8) (2007) 1808–1823.

[6] J.G. Teng, T. Yu, D. Fernando, Strengthening of steel structures with fiber-reinforced polymer composites, J. Constr. Steel Res. 78 (2012) 131–143.

[7] M.I. Alam, S. Fawzia, X.L. Zhao, A.M. Remennikov, M.R. Bambach, M. Elchalakani, Performance and dynamic behaviour of FRP strengthened CFST members subjected to lateral impact, Eng. Struct. 147 (2017) 160–176.

[8] G.D. Mancarti, Strengthening California steel bridges by prestressing, Transp. Res. Rec. 950 (1984) 183–187.

[9] A.F. Daly, W. Witarnawan, Strengthening of bridges using external post-tensioning, Proceedings of the 2nd Conf. of Eastern Asia Society for Transportation Studies, Seoul, Korea, October, 1997.

[10] T. Mimoto, I. Yoshitake, T. Sakaki, T. Mihara, Full scale flexural test of jointed concrete members strengthened with post-tension tendons with internal anchorage, Eng. Struct. 128 (2016) 139–148.

[11] E. Ben-Zvi, G. Muller, I. Rosenthal, Effect of active triaxial stress on the strength of concrete elements, Symposium on Reinforced Concrete Columns, American Concrete Institute (ACI) SP-13 1966, pp. 193–234.

[12] M.A. Bradford, H.Y. Loh, B. Uy, Slenderness limits for filled circular steel tubes, J. Constr. Steel Res. 58 (2) (2002) 243–252.

[13] M.D. Denavit, J.F. Hajjar, T. Perea, R.T. Leon, Stability analysis and design of composite structures, J. Struct. Eng. ASCE 142 (3) (2016), 04015157.

[14] L.H. Han, W. Li, R. Bjorhovde, Developments and advanced applications of concrete-filled steel tubular (CFST) structures: members, J. Constr. Steel Res. 100 (2014) 211–228.

[15] J.H. Brown, Reinforcing loaded steel compression members, AISC Eng. J. (1988) 161–168 4th Quarter.

[16] Y. Liu, L. Gannon, Finite element study of steel beams reinforced while under load, Eng. Struct. 31 (11) (2009) 2630–2642.

[17] M. Vild, M. Bajer, Strengthening under load: the effect of preload magnitudes, Proc. Eng. 161 (2016) 343–348.

[18] B. Uy, S. Das, Wet concrete loading of thin-walled steel box columns during the construction of a tall building, J. Constr. Steel Res. 42 (2) (1997) 95–119.

[19] L.H. Han, G.H. Yao, Behaviour of concrete-filled hollow structural steel (HSS) columns with pre-load on the steel tubes, J. Constr. Steel Res. 59 (2003) 1455–1475.

[20] X.X. Zha, The Theoretical and Experimental Study of the Behavior Effect on Concrete Filled Steel Tubular Members Subjected Compression-Bending-Torsion Under the Initial Stress of Steel Tube, PhD dissertation Harbin University of Civil Eng. and Architecture, Harbin, 1996 (in Chinese).

[21] F.Y. Huang, B.C. Chen, Influence of initial stress to behavior of concrete filled steel columns under axial loads, J. Fuzhou Univ. (Nat. Sci.) 36 (2) (2008) 272–277 (in Chinese).

[22] J.Y.R. Liew, D.X. Xiong, Effect of preload on the axial capacity of concrete-filled composite columns, J. Constr. Steel Res. 65 (2009) 709–722.

[23] V.I. Patel, Q.Q. Liang, M.N.S. Hadi, Behavior of biaxially-loaded rectangular concrete-filled steel tubular slender beam-columns with preload effects, Thin-Walled Struct. 79 (2014) 166–177.

[24] V.I. Patel, Q.Q. Liang, M.N.S. Hadi, Numerical analysis of circular concrete-filled steel tubular slender beam-columns with preload effects, Int. J. Struct. Stab. Dyn. 13 (3) (2013), 1250065.

[25] F. Huang, X. Yu, B. Chen, J. Li, Study on preloading reduction of ultimate load of circular concrete-filled steel tubular columns, Thin-Walled Struct. 98 (2016) 454–464.

[26] C.D. Goode, D. Lam, Concrete-filled steel tube columns – tests compared with Eurocode 4, Intl. Conf. On Composite Construction in Steel and Concrete, Composite Construction in Steel and Concrete VI 2008, pp. 317–325.

[27] CECS 77, Technical Specification for Strengthening Steel Structures, China Planning press, Beijing, 1996 (in Chinese).

[28] EN 1993-1-1+A1, Eurocode 3, Design of Steel Structures–Part 1.1: General Rules and Rules for Building, CEN, 2014.

[29] GB 50017, Standard for Design of Steel Structures, China Architecture & Building Press, Beijing, 2018 (in Chinese).

[30] JGJ/T 283, Technical Specification for Application of Self-Compacting Concrete, China Architecture & Building Press, Beijing, 2012 (in Chinese).

[31] H. Hibbitt, B. Karlsson, P. Sorensen, ABAQUS Analysis User's Manual Version 6.10, Dassault Systèmes Simulia Corp, Providence, RI, USA, 2011.

[32] F.X. Ding, X.Y. Ying, L.C. Zhou, Z.W. Yu, Unified calculation method and its application in determining the uniaxial mechanical properties of concrete, Front. Arch. Civ. Eng. China 5 (3) (2011) 381–393.

[33] F.X. Ding, J. Liu, X.M. Liu, Z.W. Yu, D.W. Li, Mechanical behavior of circular and square concrete filled steel tube stub columns under local compression, Thin-Walled Struct. 94 (2015) 155–166.

[34] F.X. Ding, C.J. Fang, Y. Bai, Y.Z. Gong, Mechanical performance of stirrup-confined concrete-filled steel tubular stub columns under axial loading, J. Constr. Steel Res. 98 (2014) 146–157.

[35] GB 50205, Code for Acceptance of Construction Quality of Steel Structures, China Planning Press, Beijing, 2002 (in Chinese).

[36] Z. Tao, B. Uy, L.H. Han, Z.B. Wang, Analysis and design of concrete-filled stiffened thin-walled steel tubular columns under axial compression, Thin-Walled Struct. 47 (12) (2009) 1544–1556.

[37] Z. Tao, Z.B. Wang, Q. Yu, Finite element modelling of concrete-filled steel stub columns under axial compression, J. Constr. Steel Res. 89 (2013) 121–131.

[38] R.D. Ziemian, Guide to Stability Design Criteria for Metal Structures, 6th ed. John Wiley & Sons, Inc, New York, 2010.

[39] N. Silvestre, D. Camotim, P.B. Dinis, Post-buckling behaviour and direct strength design of lipped channel columns experiencing local/distortional interaction, J. Constr. Steel Res. 73 (2012) 12–30.

[40] H.X. Yuan, Y.Q. Wang, L. Gardner, Y.J. Shi, Local-overall interactive buckling of welded stainless steel box section compression members, Eng. Struct. 67 (2014) 62–76.

[41] GB 50936, Technical Code for Concrete Filled Steel Tubular Structures, China Architecture & Building press, Beijing, 2014 (in Chinese).